

Three ways to improve feature alignment for open vocabulary detection

Relja Arandjelović^{1,*} Alex Andonian^{2,*},^o
 Arthur Mensch¹ Olivier J. Hénaff¹ Jean-Baptiste Alayrac¹ Andrew Zisserman^{1,3}
¹DeepMind ²MIT ³VGG, Dept. of Engineering Science, University of Oxford

Abstract

The core problem in zero-shot open vocabulary detection is how to align visual and text features, so that the detector performs well on unseen classes. Previous approaches train the feature pyramid and detection head from scratch, which breaks the vision-text feature alignment established during pretraining, and struggles to prevent the language model from forgetting unseen classes.

We propose three methods to alleviate these issues. Firstly, a simple scheme is used to augment the text embeddings which prevents overfitting to a small number of classes seen during training, while simultaneously saving memory and computation. Secondly, the feature pyramid network and the detection head are modified to include trainable gated shortcuts, which encourages vision-text feature alignment and guarantees it at the start of detection training. Finally, a self-training approach is used to leverage a larger corpus of image-text pairs thus improving detection performance on classes with no human annotated bounding boxes.

Our three methods are evaluated on the zero-shot version of the LVIS benchmark, each of them showing clear and significant benefits. Our final network achieves the new state-of-the-art on the mAP-all metric and demonstrates competitive performance for mAP-rare, as well as superior transfer to COCO and Objects365.

1. Introduction

Traditional closed vocabulary detection is limited to a fixed set of predetermined classes, and does not satisfactorily address user needs – imagine Google where you are only able to search for a predefined list of terms. Adding support for more terms requires large and costly annotation efforts, which is simply not scalable. Our objective in this paper is zero-shot open vocabulary detection, where the task is to detect any object the user queries for, in a form of a textual query (e.g. “Gargoyle”; Figure 1), even if it has not been seen during training.



Figure 1: **Zero-shot open vocabulary detection.** The detector is able to answer the queries “Gargoyle” and “Eiffel tower” despite never seeing human-annotated bounding boxes for them.

The common approach to building an open vocabulary detector is to borrow heavily from the design of standard closed vocabulary detectors (i.e. detectors capable of detecting only a fixed set of predetermined classes), and simply modify the bounding box classification procedure. Instead of producing the logits for the fixed set of classes via a fully connected layer, the score for the textual query is obtained via a scalar product between its embedding, produced by a language model, and the image region embedding, produced by the detector head. The zero-shot capability strongly relies on a good alignment between visual and textual representations – the only way queries not seen during training can be detected successfully is if the vision-text alignment holds even beyond the seen classes. In this work, we explicitly consider feature alignment and devise three ways of improving it:

(i) Many works [24, 42, 46] choose to freeze the pre-trained language model, while others, observe this yielding bad performance [26, 31, 43] and choose to train it, but with a small learning rate to prevent “catastrophic forgetting”. We also find that a frozen language model alone yields poor performance (Section 3.1.1), but propose instead to use the frozen language model together with a simple and efficient data augmentation approach, which provides superior results to both alternatives while speeding up training and decreasing accelerator memory consumption.

(ii) A typical detector pretrains the vision backbone and

*Equal contribution. ^oWork done during internship at DeepMind.

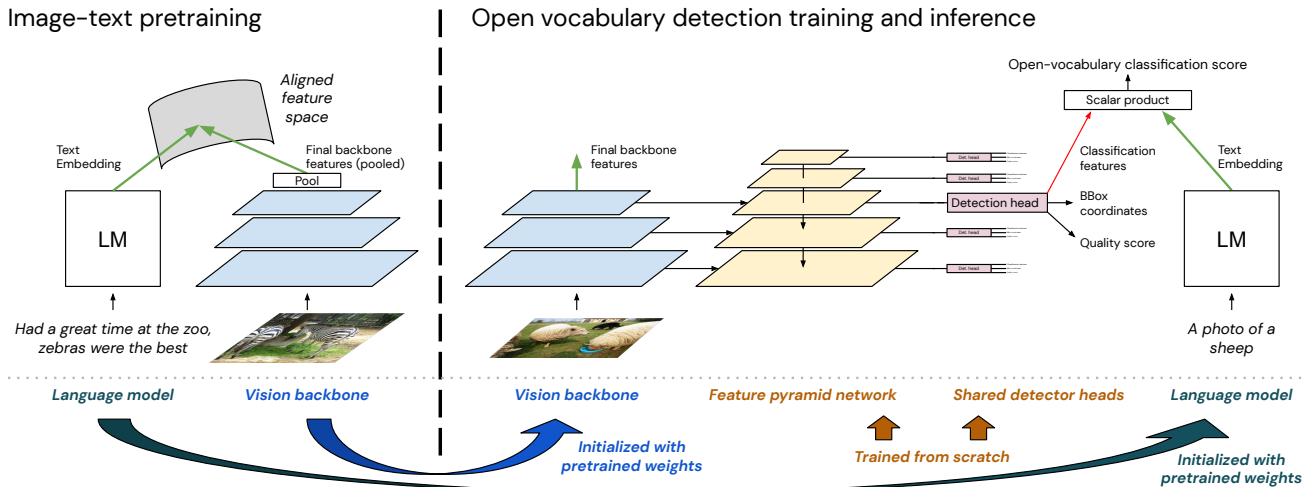


Figure 2: **A standard approach to open vocabulary detection and pretraining.** A standard single-stage detector adapted to open vocabulary detection, as explained in Section 2, makes use of a language model, vision backbone, feature pyramid network (FPN), and detector heads. The vision backbone and language model are typically pretrained in a contrastive manner, while the FPN and the detector heads are initialized from scratch.

language model on image-text datasets to obtain aligned image and text embeddings [14, 16, 31, 46], but also inserts many modules (feature pyramid network [28], detection heads [13, 28, 38]) that are trained from scratch. The added modules break the vision-text alignment established during pretraining, and we propose to side-step this issue by modifying their architecture. Explicitly, we add shortcuts and trainable gating layers which ensure the features are aligned at the start of detector training, and promote alignment throughout the training.

(iii) Feature alignment that can be achieved from relatively scarce detection training data is sparse and limited. The alignment can be improved by making use of readily available large-scale image-text data through a self-training approach [25, 37, 41, 48]. We examine self-training via pseudo-labelling in detail and observe it is crucial to use batch-negatives.

Our final approach based on all three improvements achieves the best mAP_{all} on the challenging LVIS_R benchmark, beating the next method by more than 9% points, while achieving very competitive zero-shot results and superior transfer to COCO and Objects365.

1.1. Related work

Zero-shot open vocabulary detection. Zero-shot (ZS) in the context of object detection refers to never seeing even a single annotated bounding box of the class of interest during training [31]; note that this definition allows for the existence of the object in the training set images as long as no annotations are associated with it, and it permits weak supervision, *e.g.* an image-text dataset where the object is mentioned in the text can be used as long as no bounding boxes are provided. There is a large overlap in the ZS

and open vocabulary (OV) approaches, so, confusingly, the terms are often used interchangeably, which we avoid here.

Bansal *et al.* [4] introduce ZS+OV detection where the classification layer of a closed vocabulary detector is replaced with the text embeddings of the class names, an approach taken by many subsequent works [11, 14, 16, 24, 31, 42, 46, 46], including this one. Some works [16, 24, 42] take the OV classification closer to the backbone features by directly extracting them from object proposals with ROI-Align [20], and optionally distill a strong OV classifier into the detector [16]. To improve ZS performance, Detic [46] and PromptDet [14] forego the OV aspect – knowing the names of the classes of interest (*i.e.* in evaluation: test classes) already during training enables them to obtain high-quality weak labels, and thus improve the detection performance for those classes.

Self-training is often used in the weakly- and semi-supervised settings to improve the low-shot performance of a detector [33, 34, 37, 48], by first training a detector, followed by using it to pseudo-label additional images, which are in turn used to train a better detector. This has been adapted by Detic [46] to the ZS scenario, who argue for using region proposals rather than the detector outputs to perform the pseudo-labelling. Motivated by self-supervision and contrastive learning [1, 2, 8, 19, 32, 39], we show that using batch-negatives is crucial for obtaining good performance in self-training as well.

Pretraining-preserving init. The seminal ResNet paper [21] showed the importance of shortcuts for signal propagation during training, while SkipInit [9] introduced a learnt gating that further encourages identity functions. We take most inspiration from the trainable gating of

Flamingo [1] where the vision-language model is initialized such that the visual branch is ignored, thus preserving the language model pretraining. FIBER [10] uses the Flamingo-style gating to initialize a joint vision-text encoder with pretrained dual encoders. We instead aim to preserve alignment between visual and language features obtained during pretraining but broken due to the injected detection-specific modules.

2. Baseline detector and experimental setup

In this section, we describe the baseline open vocabulary detector (Figure 2), that we build and improve upon in Section 3. We also specify the main benchmark with some implementation details, while the full details are available in Appendix A.

Open vocabulary detector. We follow the design of the single-stage FCOS detector [38], illustrated in Figure 2. It starts by processing the image with a vision backbone, features from different blocks are then passed to the feature pyramid network (FPN [28]), followed by the application of detection heads (parameters shared across levels); we use the T-Head [13] but also experiment with the classic FCOS head [38]. Each head produces dense detections associated with three quantities: bounding box coordinates, quality, and classification features. In line with other ZS/OV approaches [4, 16, 42, 46], the classification features are dotted with the embedding of the query text, obtained via a language model (LM), producing the classification logits for the given query. The final scores for all dense detections are computed by multiplying the classification probabilities with the quality scores. Non-maximum suppression [12] is then applied to produce the final detections. Training follows the standard FCOS method and its improvements, *i.e.* the dense predictions are assigned to a ground truth box or deemed as a negative through ATSS [44], and the classification, bounding box prediction, and quality prediction branches use the focal [29], gIoU [35] and IoU prediction [40] losses, respectively.

Free form textual queries are naturally supported, while it is still possible to detect a desired object class as the query text for that class (hereafter also referred to as the “class embedding”) can be produced by populating the default template (“A photo of a {*object*}”) with the class name.

Zero-shot benchmark. We use the LVIS v1.0 [18] object detection benchmark adapted for zero-shot evaluation; we call this setup LVIS_R. Following standard practice [16, 24, 46], the *rare* class annotations are removed from the training set, keeping only the *frequent* and *common* annotations (often called LVIS-base). Evaluation is then performed on all classes, reporting the box mAP for all classes (mAP_{all}) and the mAP on rare classes (mAP_{rare}), with the emphasis on mAP_{rare} as this measures the zero-shot

performance, *rare* classes playing the role of the *unseen* classes. As is best practice [17], we run all experiments with three different random seeds and report the mean and standard deviation.

Implementation details. The vision backbone and the language model are pretrained contrastively on the ALIGN [22] and LTIP datasets [1] as in [1], while the FPN and the detector head are initialized from scratch. We follow a standard training procedure for LVIS_R and tune the hyper-parameters to maximize the baseline performance; full details are listed in Appendix A. With the NFNet-F0 [6] backbone we achieve an mAP_{all} of 32.1 ± 0.31 , and mAP_{rare} of 18.9 ± 1.13 . This is a strong baseline, as for example the baseline used in a recent work [46] achieves 30.0 ± 0.4 and 16.3 ± 0.7 , respectively.

3. Three paths to alignment

In this section we describe three complementary methods for improving vision-text alignment, starting from efficient text augmentation which alleviates overfitting and facilitates large scale training (Section 3.1), followed by an architectural modification that preserves and promotes the alignment (Section 3.2), and ending with an approach for self-training which further improves the detection performance on unseen classes (Section 3.3).

3.1. Efficient text augmentation

When training a zero-shot detector, a difficult choice has to be made whether to train or to freeze the language model (LM). Many works, such as OVD [42], Detic [46] and F-VLM [24], follow the natural intuition to freeze it – the language model learnt a comprehensive textual representations during pretraining, and fine-tuning for detection on a small number of classes could make it forget about the unseen classes [31]. However, freezing it also comes with downsides – the vision model is “forced” into the language-model “mould” making it less able to adapt to the task change from pretraining which only involved global image understanding. Multiple works, such as OWL [31], GLIP [26], GLIPv2 [43], do train the language model as well, but typically use a smaller learning rate in order to prevent “catastrophic forgetting”, *e.g.* OWL [31] sets it to 1/100 of the vision model learning rate and notes poor performance when the language model is frozen.

In fact, experimentally we find that the main issue behind the poor detection performance of a system with a frozen language model is overfitting of the visual representations to the small fixed set of textual embeddings corresponding to the training classes. Augmenting of the class embeddings during training can be used as an effective way of alleviating these issues, and we consider two alternatives:

(i) *Freeze + Dropout*: despite freezing the LM, enable the

LM train or freeze	mAP _{all}	mAP _{rare}	speed	mem.
Train w/ lr-ratio 1	12.0 ± 15.9	5.2 ± 7.30	1.3	14.1G
Train w/ lr-ratio 0.01	33.2 ± 0.30	16.5 ± 0.95	1.3	14.1G
Freeze	24.4 ± 13.2	13.0 ± 8.51	1.9	10.4G
Freeze + Dropout	31.8 ± 0.20	18.7 ± 1.39	1.7	10.4G
8 Templates, infer. 1	31.3 ± 0.31	16.4 ± 1.86	2.6	9.4G
8 Templates, infer. 8	31.5 ± 0.10	17.1 ± 1.28	2.6	9.4G
80 Templates, infer. 1	31.6 ± 0.25	17.4 ± 0.38	2.6	9.6G
80 Templates, infer. 8	31.9 ± 0.06	18.1 ± 0.66	2.6	9.6G
1 Variant	16.3 ± 13.0	6.9 ± 7.89	2.6	9.4G
64 Variants	32.1 ± 0.31	18.9 ± 1.13	2.6	9.5G

Table 1: **To train or to freeze the language model (LVIS_R benchmark).** Speed is measured as the number of gradient steps per second, while ‘mem.’ denotes the peak accelerator memory usage. Methods where at least 1 out of the 3 training runs has failed are in red. Our *Freeze + Dropout* and *64 Variants* approaches perform best on the unseen classes, while speeding up training and requiring less memory.

dropout (commonly present in Transformer-based LMs during training).

(ii) *Variants*: precompute 64 variants of the class embeddings by using (i) and randomly sample a variant for each training sample.

Freezing the LM makes the training faster and simultaneously saves memory due to not having to perform backpropagation or keep the optimizer state (e.g. for popular stateful optimizers such as SGD with momentum or Adam [23]). The *Variants* approach makes it possible to completely remove the LM during training as precomputed embeddings can be used, thus making training even faster and providing further memory savings. This can be essential as detection training requires high-resolution images which for some large vision models makes it hard to fit even a batch size of 1 into the accelerator memory – it is exactly the case for our self-training NFNet-F6 experiments (Section 3.3) which are not possible without the *Variants* method.

3.1.1 Results

All experiments are performed on the LVIS_R benchmark (c.f. Section 2). The effect of different approaches to training or freezing the language model are shown in Table 1.

Training the LM with the same learning rate as the vision model is unstable and results in poor performance. Using the OWL [31] strategy of training the LM with a very small learning rate yields good performance on all classes. However, when compared with our augmentation approaches, it becomes clear that it is underperforming on unseen classes, as even this small learning rate causes some forgetting, albeit arguably not “catastrophic”.

Freezing the LM underperforms and is unstable, testifying to overfitting; this is equivalent to the *1 Variant* scenario which performs equally badly. However, simply using dropout while keeping the network frozen performs very well – achieving the best mAP on the unseen classes. Furthermore, the *64 Variants* approach, where the variants of the class embeddings are precomputed and sampled during training, performs equally well while enabling us to remove the LM inference from training. This in turn achieves a 9% reduction in memory use and a speedup of 53% vs *Freeze + Dropout*, and 33% memory savings and a 2× speedup vs the LM-training approaches.

Templates. An alternative to the *Variants* approach is to use many different text templates (e.g. “A close-up photo of the {object}” or “A low resolution photo of the {object}”) to compute the class embeddings and randomly sample them for each training sample [31]. The 8 templates are formed by combining the “7 best” CLIP templates [32] and the default one (“A photo of a {object}”), while the 80 templates are the CLIP 80 templates (the default is already included). The use of multiple templates during training has a similar effect to *64 Variants* in that it trains stably and outperforms the LM-training approaches. However, for good performance it requires inference with multiple templates [31] (i.e. class probabilities are averaged across the different templates) which increases complexity and inference memory requirements, while still being beaten by our simple *Variants* approach. We hypothesise this is because the templates have been designed for ImageNet classification and contain obscure concepts such as “An origami {object}”. It is not easy to design many good templates, so our approach to simply compute *64 Variants* of the class embedding by using the natural default template and enabling dropout is more effective.

3.2. Alignment preserving architecture

As outlined in Section 1 and shown in Figure 2, a typical setup that we also follow is to: (1) pretrain a vision-language model, (2) construct the open-vocabulary detector by re-using the vision and text backbones and adding detection-specific layers (feature pyramid network (FPN) and detector heads), (3) initialize the backbones from (1) while initializing the rest (FPN, heads) from scratch, and (4) train all or subsets of parameters e.g. freezing the LM backbone.

The disconnect between steps (1) and (3) stands out – the vision and language backbones were trained together to produce aligned representations of their respective modalities, and we sever that alignment by introducing many layers in-between that are trained from scratch. The detector training then spends a long time seeking to realign the features, and it is very likely that during this initial chaos some of the pre-trained alignment is forever lost. Here we introduce small

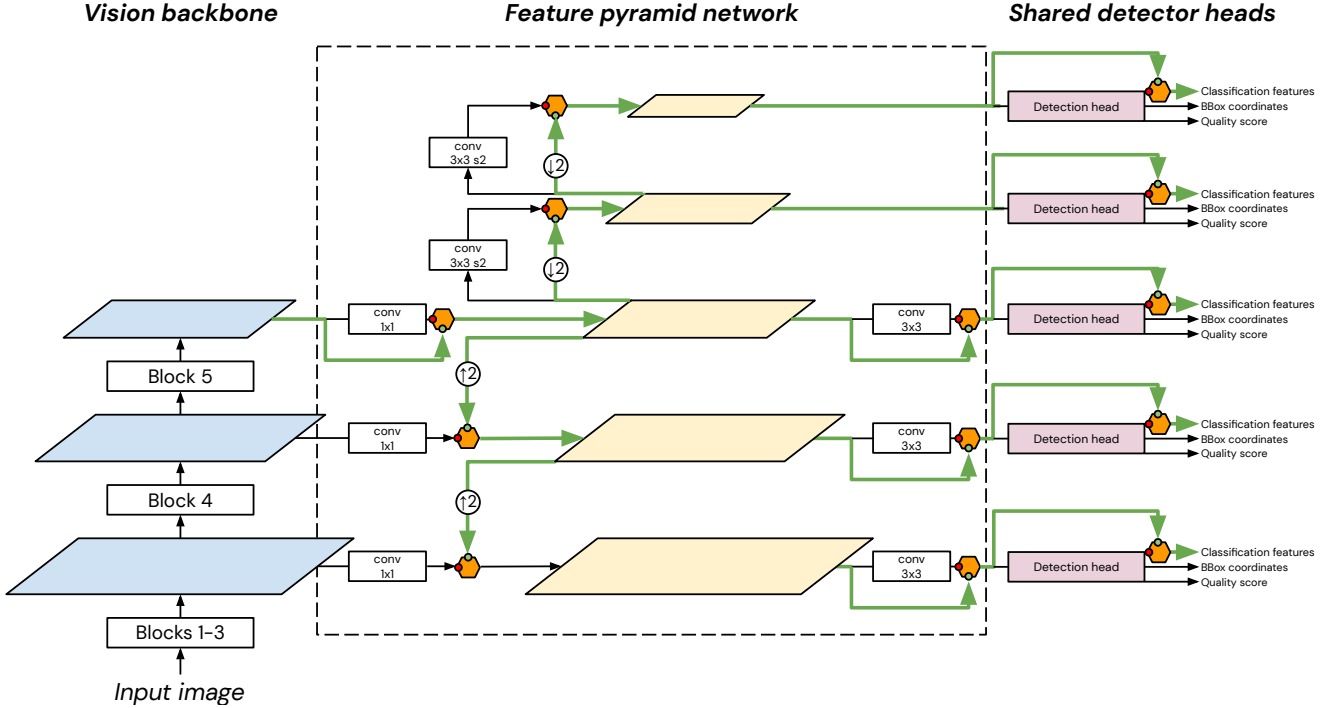


Figure 3: **Alignment preserving architecture (APA)**. The standard single-stage object detector architecture [Backbone \rightarrow Feature pyramid network (FPN) \rightarrow Detector heads] is augmented with shortcuts and trainable gating layers (\odot), which at init propagate the green input and block the red input. The output is computed as $x(1 - \tan \alpha) + y \tan \alpha$, and $\alpha = 0$ at init. The green arrows show the propagation of the last backbone features at init all the way to the final detector head classification features. Light blue and light yellow parallelograms represent the backbone and FPN feature maps, respectively; circles with $\uparrow 2$ and $\downarrow 2$ are non-trainable up- and down-sampling, squares are trainable modules (e.g. convolutions), and \odot are the trainable gates; convolution blocks show the kernel size and potential striding ('s2': stride 2). The standard architecture (i.e. without the shortcuts and gates) is shown in the supplementary material.

architectural changes to the detector-specific layers which serve to maintain the alignment of vision-text features at the start, and promote it throughout the detector training.

The architectural modifications are shown in Figure 3 and consist of strategically adding shortcut connections and trainable gating layers [1]. A trainable gating layer, with inputs x and y and a trainable scalar parameter α , produces the output $o = x(1 - \tan \alpha) + y \tan \alpha$, where α is initialized to 0 meaning $o = x$ at the start of training. The shortcuts and gates are added such that at the start of training, the features from the end of the vision backbone are “forwarded” through the FPN and detector heads all the way to the final classification features. In other words, at the start of training, the detector head classification features at all levels of the pyramid are equal to the backbone features. Recall that the vision and text backbones have been pretrained for alignment. This means that due to the specific gated-shortcut architecture and initialization, the detection head classification features (now equal to the backbone features) are already aligned with the text embeddings at the beginning of detector training. Thus, the training is improved as

it starts from a good initial guess for the object classification and only needs to learn to improve the classification and bounding box prediction, rather than spend effort in re-discovering the vision-text alignment.

Aligned architecture design. Here we explain in more detail the recipe for converting an architecture to its gated-shortcut version. As explained above, the overall aim is to forward the final backbone features (as they are pretrained to be aligned with the text embeddings) to the end of the detection head. So one only needs to follow the “flow” of the final backbone features and apply the following operations: (i) if they are mixed with another signal, add a gate that zeroes-out the second signal at the start of training, (ii) if an alignment preserving operation is performed (e.g. upsampling) do nothing, (ii) if an alignment damaging transformation is performed (e.g. a convolution), make a shortcut connection and add a gate such that the output equals the shortcut at the start of training.

These principles and the resulting architecture are illustrated in Figure 3, where the FPN is augmented with the shortcuts and gates, while a single shortcut+gate combina-

Architecture		APA		LVIS _R performance	
Backb.	Head	FPN	Head	mAP _{all}	mAP _{rare}
NF-F0	FCOS			30.4 ± 0.21	16.1 ± 1.46
NF-F0	FCOS	✓	✓	32.7 ± 0.15	19.8 ± 0.34
NF-F0	T-Head			32.1 ± 0.31	18.9 ± 1.13
NF-F0	T-Head	✓		32.4 ± 0.44	18.3 ± 1.58
NF-F0	T-Head		✓	33.3 ± 0.15	19.6 ± 0.49
NF-F0	T-Head	✓	✓	33.8 ± 0.15	20.9 ± 0.34
NF-F6	T-Head			41.6 ± 0.17	21.1 ± 0.40
NF-F6	T-Head	✓	✓	43.5 ± 0.12	27.6 ± 0.80

Table 2: **Alignment preserving architecture (APA)**. All networks were trained with the *64 Variants* approach (Section 3.1). The added shortcuts and trainable gating layers consistently improve the detection performance for both the backbone and detection head architectures.

tion is used around the entire detector head. This makes it easy to apply the design to different detector heads (*e.g.* FCOS [38] vs T-Head [13]) which contain potentially more complex operations.

3.2.1 Results

Table 2 shows the results of our the alignment preserving architectures (APA).

Alignment preserving vs vanilla architecture. Coupled with the NFNet-F0 vision backbone and the FCOS [38] detector head, our design improves mAP_{all} and mAP_{rare} by +2.3% and +3.7%, respectively. Similarly, for the better performing T-Head [13] APA achieves +1.7% and +2%, respectively. It is impressive that the improvements transfer to the larger NFNet-F6 network which already exhibits an excellent mAP_{all} of 41.6%, which is further boosted by APA by +1.9% to reach 43.5%. The largest improvement can be observed for mAP_{rare} where the alignment preserving architecture tops the strong baseline by +6.5% and yields 27.6%.

In the FPN, Head or everywhere? Table 2 shows it is more important to apply APA onto the detection head than the FPN – we speculate that this is because the detection head is much deeper and therefore without APA it takes longer to learn to re-learn the feature alignment in the detector head than in the FPN. However, applying APA onto both simultaneously clearly dominates, confirming our intuition that maintaining alignment from the very start of training is important.

3.3. Self-training

Text augmentation (Section 3.1) and the alignment preserving architecture (Section 3.2) bring significant gains in zero-shot performance due to the improved feature align-

ment. However, it is still ambitious to ask for the detector to extrapolate to completely unseen classes. In this section, we investigate how to use self-training via pseudo-labelling to further improve the feature alignment beyond the seen classes.

We propose a simple three-stage approach. First, a good open vocabulary detector is trained using the previous two improvements (Sections 3.1 and 3.2), called *2Ways*. The detector is then used to pseudo-label an additional dataset that contains only images-text pairs scraped from the internet, *i.e.* it contains weak image-level information (the text), without any human supervision nor finer-grained annotations such as classes, bounding boxes or segmentations. The detector uses the text embedding of the entire caption as the object query, and we simply use the single highest scoring box per image if it passes a confidence threshold of 0.25. Finally, a new, stronger, open vocabulary detector (*3Ways*) is trained by combining the strongly supervised data (LVIS_R) and the pseudo-labelled dataset, and treating the pseudo-labels as ground truth.

It is worth elaborating on the exact details of the final training stage. Recall from Section 2 that for training with the true ground truth annotations, we follow the standard training procedure; *i.e.*, certain detector head classification features are assigned to be positives for particular classes (in the open vocabulary case, its text embedding) based on their pyramid level and location in the feature map [44]. The same features are negatives for other classes, and all remaining features are negatives for all classes. For example, if an image has a *dog* in it and no *cat*, we have: (i) some features depending on scale and location are positives for *dog*, (ii) features that are not positives for *dog* are negatives for *dog*, (iii) all features are negatives for *cat*. Training then proceeds with the standard per-class binary focal loss [29].

We propose an analogous mechanism when training with the pseudo-labels. The single pseudo-bounding box per image is deemed to correspond to the entire caption, and other captions in the batch are used as negatives. Therefore, for the *i*-th image in the batch, we have: (i) some features are deemed positive for the *i*-th caption again following [44], (ii) features that are not positive are negatives for the *i*-th caption, (iii) all features are negatives for the *j*-th caption where $i \neq j$; we call this the use of “batch-negatives”. The same binary focal loss is used for training. As will be shown in Section 3.3.1 and is commonly observed in the self-supervised literature [2, 8, 19, 39], batch-negatives are crucial to obtain good performance.

Relation to other methods. While multiple works have used self-training with pseudo-labelling to boost the detector performance, none follow the above approach. Pseudo-labelling is popular in the weakly-supervised (classes in the image are specified but not their location) or semi-supervised low-shot works [33, 34, 37, 48] with closed vo-

Self-training method	Backb.	mAP _{all}	mAP _{rare}
2Ways (no self-training)	NF-F0	33.8 \pm 0.15	20.9 \pm 0.34
Image bbox w/o batch-negs	NF-F0	33.9 \pm 0.30	20.9 \pm 1.06
Image bbox	NF-F0	35.1 \pm 0.26	24.2 \pm 1.37
Detic [46] open-voc. [†]	NF-F0	34.8 \pm 0.32	23.4 \pm 1.49
3Ways w/o batch-negs	NF-F0	34.2 \pm 0.15	20.7 \pm 0.35
3Ways	NF-F0	35.7 \pm 0.20	25.6 \pm 1.12
2Ways (no self-training)	NF-F6	43.5 \pm 0.12	27.6 \pm 0.80
3Ways	NF-F6	44.6 \pm 0.31	30.1 \pm 1.83

Table 3: **Self-training (LVIS_R benchmark).** CC12M is pseudo-labelled with the 2Ways detector (Sections 3.1 and 3.2). Detic[†] is our reimplementation of Detic [46], Image bbox uses the entire image as the pseudo-detection while 3Ways uses the 2Ways’s best prediction; Section 3.3 explains all methods. Self-training helps, and batch-negatives are important.

cabulary detectors. This means that pseudo-labelling is easier as all classes are seen during training, but also that the self-training follows exactly the same setup as the initial training, where the negatives are other classes and there is no need or way to use batch-negatives.

Our 3Ways uses the pseudo-detections from the 2Ways detector conditioned on the image caption, while Detic [46] computes the pseudo-detection independently of the caption by taking the largest bounding box proposal. Detic adopts batch-negatives but does so on the image-level rather than the bounding box-level; a more detailed discussion is available in Appendix C. GLIPv2 [43] also uses batch-negatives, but does not consider the zero-shot scenario. While we use the entire caption at once to produce pseudo-detections, GLIPv2 extracts noun phrases and pseudo-labels them individually. This could provide better quality pseudo-labels, but comes with its downsides as well, in that it depends on the quality of the text parser and requires additional book-keeping and special handling of repeated noun phrases in the batch.

3.3.1 Results

Implementation details. We start from the strong 2Ways detector from Section 3.2 and verify that longer training on LVIS_R does not improve results further. Conceptual Captions 12M [7] (CC12M), an image-caption dataset gathered automatically from the internet containing 12M images, is used for all self-training experiments. The self-training starts from the 2Ways detector checkpoint and continues training, where each training step simultaneously optimizes the losses on a batch of LVIS_R images with true ground-truth and a batch of pseudo-labelled images from CC12M. In line with [46], we find we can reduce the resolution of the CC12M images (for LVIS_R we use 800 × 1024, while for

CC12M 400 × 512 is sufficient) thus fitting a larger number of images in the batch and allowing for more batch-negatives.

Performance. Table 3 shows the self-training results – it is clear that our self-training, 3Ways, significantly improves both metrics and on both backbones, providing an especially large boost for the unseen classes.

Comparison to Detic [46]. We do not simply copy the numbers from [46] as this wouldn’t be a fair comparison – we use different visual backbones, detector type, the self-training dataset, *etc.* Furthermore, Detic [46] focuses on the zero-shot and not open-vocabulary aspect (*e.g.* the full approach specifically searches for the LVIS-rare classes in the captions and uses this as the pseudo-label). Therefore, we reimplement the open-vocabulary version of Detic[†], using our 2Ways detector (see Appendix C). Detic[†] performs well, giving improvements over 2Ways. However, our self-training approach also significantly beats Detic[†]. We also compare to another approach proposed by [46] where the pseudo-detection is simply taken to be the image bounding box. In fact, *Image bbox* beats Detic[†] slightly, but 3Ways is still superior.

Importance of batch-negatives. As an ablation, we also train versions of the *Image bbox* and our 3Ways approaches where batch-negatives are not used. The results show a clear large benefit of using batch-negatives – without them there is barely any gain from self-training as the task is too easy.

4. Results and discussion

Comparison on an equal footing with the state-of-the-art is hard because most works use different visual backbones, pretraining, detector architecture, training procedure, augmentations, *etc.* Sections 3.1.1, 3.2.1 and 3.3.1 demonstrate the performance of each of our methods individually through fair comparisons where all these aspects are identical, while here we resort to the standard practice of reporting system-level performance (Table 4). We list best performing methods that are truly zero-shot and open vocabulary, and are trained following the LVIS_R benchmark rules (*i.e.* the only detection annotations used are the LVIS training set with the rare classes removed). For example, this criterion disqualifies PromptDet [14] and the best performing versions of Detic [46] (they actively use the list of LVIS classes to pseudo-label additional images, *i.e.* not open vocabulary), FIBER [10] and some OWL [31] experiments (train on many more detection annotations), GLIP [26] and GLIPv2 [43] (rare classes are not removed during training so not zero-shot, and more training data is used), *etc.*

Our final open vocabulary detector, 3Ways, achieves the highest mAP_{all} and competitive mAP_{rare}. On mAP_{all} it sets the state-of-the-art by a large margin – the largest network (NFNet-F6 with 440M parameters) achieves 44.6%

Method	Backbone	#Params	Self-training	mAP _{all}	mAP _{rare}	mAP _{comm}	mAP _{freq}
Detic [46] open-voc. ^(m)	R50	26M	✓	30.4	17.4		
DetPro [11]	R50	26M		28.4	20.8	27.8	32.4
RegionCLIP [45]	R50x4	87M	✓	32.1	22.0	32.1	36.9
OWL [31]	VIT-L/14	303M		34.7	25.6		
OWL [31]	VIT-H/14	627M		35.3	23.3		
F-VLM [24]	R50x4	87M		28.5	26.3		
F-VLM [24]	R50x64	420M		34.9	32.8		
0Ways [this work]	NFNet-F0	71M		16.3 ± 13.0	6.9 ± 7.89	13.2 ± 11.3	23.7 ± 11.7
1Ways [this work]	NFNet-F0	71M		32.1 ± 0.31	18.9 ± 1.13	29.5 ± 0.15	40.9 ± 0.08
2Ways [this work]	NFNet-F0	71M		33.8 ± 0.15	20.9 ± 0.34	32.4 ± 0.20	41.0 ± 0.05
3Ways [this work]	NFNet-F0	71M	✓	35.7 ± 0.20	25.6 ± 1.12	34.2 ± 0.05	41.8 ± 0.02
0Ways [this work]	NFNet-F6	440M		0.8 ± 0.19	0.4 ± 0.12	0.7 ± 0.16	1.0 ± 0.24
1Ways [this work]	NFNet-F6	440M		41.6 ± 0.17	21.1 ± 0.40	42.9 ± 0.19	49.2 ± 0.09
2Ways [this work]	NFNet-F6	440M		43.5 ± 0.12	27.6 ± 0.80	44.9 ± 0.10	48.8 ± 0.01
3Ways [this work]	NFNet-F6	440M	✓	44.6 ± 0.31	30.1 ± 1.83	46.0 ± 0.17	49.3 ± 0.08

Table 4: **State-of-the-art for zero-shot open vocabulary detection on LVIS_R**. ^(m) denotes that Detic [46] only reports the mask mAPs, box mAP should not be much higher. *0Ways*, *1Ways*, *2Ways* and *3Ways* refer to the baseline detector with the frozen LM and no text augmentation, and cumulative application of our three methods from Sections 3.1, 3.2 and 3.3, respectively. *3Ways* performs well, yielding the best mAP_{all} by a large margin and achieving a favourable mAP_{rare}.

(and 43.5% without self-training) while the best second is at 35.3% (OWL [31]’s VIT-H/14 with 630M parameters), making for an impressive improvement of 9.3% points (8.2% without self-training). Even our smaller network (NFNet-F0 with 71M parameters) with self-training beats the previously best reported performance.

On the unseen classes, mAP_{rare}, we compare favourably to the latest approaches. Only the concurrent F-VLM [24] method performs better, achieving 32.8% for the largest R50x64 model, while our equally large NFNet-F6 is a close second at 30.1%. It should be noted that, when trained on full LVIS, it has been observed that mAP_{rare} inherently has high variance as these are the long tail categories, and an absolute difference of 1% might not be significant [17]; for example, our best performing run achieves 31.7%. The shared third place with a significantly lower mAP_{rare} value of 25.6% is achieved by OWL with VIT-L/14 (310M parameters) and our much smaller NFNet-F0 model (71M parameters).

The good performance is partially due to the use of the strong vision backbone. However, simply using it out of the box (*0Ways*) fails (Table 4, c.f. Section 3.1.1) and our methods are required to unlock its power.

Transfer capabilities are tested by evaluating the LVIS_R trained networks on COCO [27] and Objects365-v1 [36]. Table 5 shows the networks achieve impressive performance: on COCO even our smallest model without self-training beats all previous approaches, while on Objects365 (estimated by [24] to have only 63% overlap with LVIS_R training classes) *3Ways* improves upon the previous best mAP by 5.1% points.

Method	Backbone	#Params	COCO	O365
ViLD [16]	R50	26M	36.6	11.8
DetPro [11]	R50	26M	34.9	12.1
F-VLM [24]	R50x4	87M	36.0	14.2
F-VLM [24]	R50x64	420M	39.8	17.7
2Ways [this work]	NF-F0	71M	40.6	14.6
3Ways [this work]	NF-F0	71M	41.5	16.4
2Ways [this work]	NF-F6	440M	46.5	20.3
3Ways [this work]	NF-F6	440M	46.9	22.8

Table 5: **Transfer**. The LVIS_R trained networks are evaluated on COCO [27] and Objects365-v1 [36] without any additional training.

Qualitative results are provided in Appendix D.

5. Conclusions

We introduced three methods for improving alignment between visual and text features, which in turn boosts zero-shot detection performance. They reduce overfitting and forgetting of concepts learnt during pretraining, improve training speed while decreasing accelerator memory requirements, and make use of large image-text datasets without costly detection annotations. We achieve superior mAP_{all} on the challenging LVIS_R benchmark, and transfer to COCO and Objects365, while obtaining mAP_{rare} competitive with concurrent work. Further research directions include investigating how to even more efficiently make use of plentiful image-text data with improved pseudo-labelling, losses, or combinations with self-supervised learning.

Acknowledgments. We thank Evan Shelhamer for fruitful discussions and Iain Barr for help with the codebase.

References

- [1] Jean-Baptiste Alayrac, Jeff Donahue, Pauline Luc, Antoine Miech, Iain Barr, Yana Hasson, Karel Lenc, Arthur Mensch, Katie Millican, Malcolm Reynolds, Roman Ring, Eliza Rutherford, Serkan Cabi, Tengda Han, Zhitao Gong, Sina Samangooei, Marianne Monteiro, Jacob Menick, Sebastian Borgeaud, Andrew Brock, Aida Nematzadeh, Sahand Sharifzadeh, Mikolaj Binkowski, Ricardo Barreira, Oriol Vinyals, Andrew Zisserman, and Karen Simonyan. Flamingo: a visual language model for few-shot learning. In *NeurIPS*, 2022. [2](#), [3](#), [5](#), [11](#)
- [2] Relja Arandjelović and Andrew Zisserman. Look, listen and learn. In *Proc. ICCV*, 2017. [2](#), [6](#)
- [3] Igor Babuschkin, Kate Baumli, Alison Bell, Surya Bhupatiraju, Jake Bruce, Peter Buchlovsky, David Budden, Trevor Cai, Aidan Clark, Ivo Danihelka, Claudio Fantacci, Jonathan Godwin, Chris Jones, Tom Hennigan, Matteo Hessel, Steven Kapturowski, Thomas Keck, Iurii Kemaev, Michael King, Lena Martens, Vladimir Mikulik, Tamara Norman, John Quan, George Papamakarios, Roman Ring, Francisco Ruiz, Alvaro Sanchez, Rosalia Schneider, Eren Sezener, Stephen Spencer, Srivatsan Srinivasan, Wojciech Stokowiec, and Fabio Viola. The DeepMind JAX ecosystem, 2020. [11](#)
- [4] Ankan Bansal, Karan Sikka, Gaurav Sharma, Rama Chellappa, and Ajay Divakaran. Zero-shot object detection. In *Proc. ECCV*, 2018. [2](#), [3](#)
- [5] James Bradbury, Roy Frostig, Peter Hawkins, Matthew James Johnson, Chris Leary, Dougal Maclaurin, George Necula, Adam Paszke, Jake VanderPlas, Skye Wanderman-Milne, and Qiao Zhang. JAX: Composable transformations of Python+NumPy programs, 2018. [11](#)
- [6] Andrew Brock, Soham De, Samuel L. Smith, and Karen Simonyan. High-performance large-scale image recognition without normalization. *arXiv preprint arXiv:2102.06171*, 2021. [3](#), [10](#)
- [7] Soravit Changpinyo, Piyush Sharma, Nan Ding, and Radu Soricut. Conceptual 12M: Pushing web-scale image-text pre-training to recognize long-tail visual concepts. In *Proc. CVPR*, 2021. [7](#)
- [8] Ting Chen, Simon Kornblith, Mohammad Norouzi, and Geoffrey Hinton. A simple framework for contrastive learning of visual representations. In *Proc. ICML*, 2020. [2](#), [6](#)
- [9] Soham De and Samuel L. Smith. Batch normalization biases residual blocks towards the identity function in deep networks. In *NeurIPS*, 2020. [2](#)
- [10] Zi-Yi Dou, Aishwarya Kamath, Zhe Gan, Pengchuan Zhang, Jianfeng Wang, Linjie Li, Zicheng Liu, Ce Liu, Yann LeCun, Nanyun Peng, Jianfeng Gao, and Lijuan Wang. Coarse-to-fine vision-language pre-training with fusion in the backbone. In *NeurIPS*, 2022. [3](#), [7](#)
- [11] Yu Du, Fangyun Wei, Zihe Zhang, Miaojing Shi, Yue Gao, and Guoqi Li. Learning to prompt for open-vocabulary object detection with vision-language model. In *Proc. CVPR*, 2022. [2](#), [8](#)
- [12] Pedro F. Felzenszwalb, Ross B. Girshick, David McAllester, and Deva Ramanan. Object detection with discriminatively trained part-based models. *IEEE PAMI*, 32(9):1627–1645, 2010. [3](#)
- [13] Chengjian Feng, Yujie Zhong, Yu Gao, Matthew R. Scott, and Weilin Huang. TOOD: Task-aligned one-stage object detection. In *Proc. ICCV*, 2021. [2](#), [3](#), [6](#), [10](#)
- [14] Chengjian Feng, Yujie Zhong, Zequn Jie, Xiangxiang Chu, Haibing Ren, Xiaolin Wei, Weidi Xie, and Lin Ma. Prompt-Det: Towards open-vocabulary detection using uncurated images. In *Proc. ECCV*, 2022. [2](#), [7](#)
- [15] Golnaz Ghiasi, Yin Cui, Aravind Srinivas, Rui Qian, Tsung-Yi Lin, Ekin D. Cubuk, Quoc V. Le, and Barret Zoph. Simple copy-paste is a strong data augmentation method for instance segmentation. In *Proc. CVPR*, 2021. [10](#)
- [16] Xiuye Gu, Tsung-Yi Lin, Weicheng Kuo, and Yin Cui. Open-vocabulary object detection via vision and language knowledge distillation. In *Proc. ICLR*, 2022. [2](#), [3](#), [8](#)
- [17] Agrim Gupta, Piotr Dollár, and Ross Girshick. LVIS best practices. <https://www.lvisdataset.org/bestpractices>. [3](#), [8](#)
- [18] Agrim Gupta, Piotr Dollár, and Ross Girshick. LVIS: A dataset for large vocabulary instance segmentation. In *Proc. CVPR*, 2019. [3](#)
- [19] Kaiming He, Haoqi Fan, Yuxin Wu, Saining Xie, and Ross Girshick. Momentum contrast for unsupervised visual representation learning. In *Proc. CVPR*, 2020. [2](#), [6](#)
- [20] Kaiming He, Georgia Gkioxari, Piotr Dollár, and Ross Girshick. Mask R-CNN. In *Proc. ICCV*, 2017. [2](#)
- [21] Kaiming He, Xiangyu Zhang, Shaoqing Ren, and Jian Sun. Deep residual learning for image recognition. In *Proc. CVPR*, 2016. [2](#)
- [22] Chao Jia, Yinfei Yang, Ye Xia, Yi-Ting Chen, Zarana Parekh, Hieu Pham, Quoc V. Le, Yunhsuan Sung, Zhen Li, and Tom Duerig. Scaling up visual and vision-language representation learning with noisy text supervision. In *Proc. ICML*, 2021. [3](#)
- [23] Diederik P. Kingma and Jimmy Ba. Adam: A method for stochastic optimization. In *Proc. ICLR*, 2015. [4](#)
- [24] Weicheng Kuo, Yin Cui, Xiuye Gu, AJ Piergiovanni, and Anelia Angelova. F-VLM: Open-vocabulary object detection upon frozen vision and language models. In *Proc. ICLR*, 2023. [1](#), [2](#), [3](#), [8](#), [13](#)
- [25] Dong-Hyun Lee. Pseudo-label: The simple and efficient semi-supervised learning method for deep neural networks. In *ICML Workshop*, 2013. [2](#)
- [26] Liunian Harold Li, Pengchuan Zhang, Haotian Zhang, Jianwei Yang, Chunyuan Li, Yiwu Zhong, Lijuan Wang, Lu Yuan, Lei Zhang, Jenq-Neng Hwang, Kai-Wei Chang, and Jianfeng Gao. Grounded language-image pre-training. In *Proc. CVPR. IEEE*, 2022. [1](#), [3](#), [7](#)
- [27] Tsung-Yi Lin, Michael Maire, Serge J. Belongie, Lubomir D. Bourdev, Ross B. Girshick, James Hays, Pietro Perona, Deva Ramanan, Piotr Dollár, and C. Lawrence Zitnick. Microsoft COCO: Common objects in context. In *Proc. ECCV*, 2014. [8](#)
- [28] Tsung-Yi Lin, Piotr Dollár, Ross Girshick, Kaiming He, Bharath Hariharan, and Serge Belongie. Feature pyramid networks for object detection. In *Proc. CVPR*, 2017. [2](#), [3](#), [11](#)
- [29] Tsung-Yi Lin, Priya Goyal, Ross Girshick, Kaiming He, and Piotr Dollár. Focal loss for dense object detection. In *Proc.*

- CVPR, 2017. 3, 6, 10
- [30] Ilya Loshchilov and Frank Hutter. Decoupled weight decay regularization. In *Proc. ICLR*, 2019. 10
- [31] Matthias Minderer, Alexey Gritsenko, Austin Stone, Maxim Neumann, Dirk Weissenborn, Alexey Dosovitskiy, Aravindh Mahendran, Anurag Arnab, Mostafa Dehghani, Zhuoran Shen, Xiao Wang, Xiaohua Zhai, Thomas Kipf, and Neil Houlsby. Simple open-vocabulary object detection with vision transformers. In *Proc. ECCV*, 2022. 1, 2, 3, 4, 7, 8, 10
- [32] Alec Radford, Jong Wook Kim, Chris Hallacy, Aditya Ramesh, Gabriel Goh, Sandhini Agarwal, Girish Sastry, Amanda Askell, Pamela Mishkin, Jack Clark, Gretchen Krueger, and Ilya Sutskever. Learning transferable visual models from natural language supervision. *arXiv preprint arXiv:2103.00020*, 2021. 2, 4
- [33] Vignesh Ramanathan, Rui Wang, and Dhruv Mahajan. DLWL: Improving detection for lowshot classes with weakly labelled data. In *Proc. CVPR*, 2020. 2, 6, 11
- [34] Joseph Redmon and Ali Farhadi. YOLO9000: Better, faster, stronger. In *Proc. CVPR*, 2017. 2, 6, 11
- [35] Hamid Rezaatoughi, Nathan Tsoi, JunYoung Gwak, Amir Sadeghian, Ian Reid, and Silvio Savarese. Generalized intersection over union: A metric and a loss for bounding box regression. In *Proc. CVPR*, 2019. 3, 10
- [36] Shuai Shao, Zeming Li, Tianyuan Zhang, Chao Peng, Gang Yu, Xiangyu Zhang, Jing Li, and Jian Sun. Objects365: A large-scale, high-quality dataset for object detection. In *Proc. ICCV*, 2019. 8
- [37] Kihyuk Sohn, Zizhao Zhang, Chun-Liang Li, Han Zhang, Chen-Yu Lee, and Tomas Pfister. A simple semi-supervised learning framework for object detection. *arXiv preprint arXiv:2005.04757*, 2020. 2, 6, 11
- [38] Zhi Tian, Chunhua Shen, Hao Chen, and Tong He. FCOS: Fully convolutional one-stage object detection. In *Proc. ICCV*, 2019. 2, 3, 6, 11
- [39] Aäron van den Oord, Yazhe Li, and Oriol Vinyals. Representation learning with contrastive predictive coding. *arXiv preprint arXiv:1807.03748*, 2018. 2, 6
- [40] Shengkai Wu, Xiaoping Li, and Xinggang Wang. IoU-aware single-stage object detector for accurate localization. *Image and Vision Computing*, 2020. 3, 10
- [41] Qizhe Xie, Minh-Thang Luong, Eduard Hovy, and Quoc V. Le. Self-training with noisy student improves imagenet classification. In *Proc. CVPR*, 2019. 2
- [42] Alireza Zareian, Kevin Dela Rosa, Derek Hao Hu, and Shih-Fu Chang. Open-vocabulary object detection using captions. In *Proc. CVPR*, 2021. 1, 2, 3
- [43] Haotian Zhang, Pengchuan Zhang, Xiaowei Hu, Yen-Chun Chen, Liunian Harold Li, Xiyang Dai, Lijuan Wang, Lu Yuan, Jenq-Neng Hwang, and Jianfeng Gao. GLIPv2: Unifying localization and vision-language understanding. In *NeurIPS*, 2022. 1, 3, 7, 11
- [44] Shifeng Zhang, Cheng Chi, Yongqiang Yao, Zhen Lei, and Stan Z. Li. Bridging the gap between anchor-based and anchor-free detection via adaptive training sample selection. In *Proc. CVPR*, 2020. 3, 6
- [45] Yiwu Zhong, Jianwei Yang, Pengchuan Zhang, Chunyuan Li, Noel Codella, Liunian Harold Li, Luwei Zhou, Xiyang Dai, Lu Yuan, Yin Li, and Jianfeng Gao. RegionCLIP: Region-based language-image pretraining. In *Proc. CVPR*, 2022. 8
- [46] Xingyi Zhou, Rohit Girdhar, Armand Joulin, Philipp Krähenbühl, and Ishan Misra. Detecting twenty-thousand classes using image-level supervision. In *Proc. ECCV*, 2022. 1, 2, 3, 7, 8, 11, 12
- [47] Xingyi Zhou, Vladlen Koltun, and Philipp Krähenbühl. Probabilistic two-stage detection. *arXiv preprint arXiv:2103.07461*, 2021. 10
- [48] Barret Zoph, Golnaz Ghiasi, Tsung-Yi Lin, Yin Cui, Hanxiao Liu, Ekin D. Cubuk, and Quoc V. Le. Rethinking pre-training and self-training. In *NeurIPS*, 2020. 2, 6, 11

Appendix overview

Appendix A contains full details of the detector architecture and training procedure, while Appendix B provides more information on the alignment preserving architecture. In Appendix C we give further details on the implementation of self-training, reimplementing of Detic, and relation to other methods. Finally, qualitative detection examples are shown in Appendix D.

A. Implementation details

Architecture. For closed vocabulary detectors, the final fully connected layer also trains a per-class bias, and initializing it according to the focal loss scheme [29] stabilizes the beginning of training. For the open vocabulary case it is not possible to have this per-class bias term, so we use a learnt shared bias, *i.e.* a single scalar added to the scalar product between the classification features and the text embeddings, initialized in the same way, *i.e.* $\text{bias}_{\text{init}} = -\log((1-p)/p)$, where $p = 0.01$. In initial experiments we observed this indeed aided stability.

The original T-Head detector head architecture [13] uses the “task-aligned predictor” (TAP) only on the regression and classification branches and not on the quality branch. For consistency we simply use TAP on all three branches.

Input and annotation processing. Training and evaluation is done with 800×1024 images for all datasets (LVIS_R, COCO, Objects365) apart from the pseudo-labelled images from CC12M where we found that 400×512 is sufficient. Training uses large scale jittering [15] for LVIS_R and small scale jittering for CC12M. Following [31, 47], 50 pseudo-negatives are used for each training sample.

Total loss is the sum of three equally weighted standard losses: binary focal loss [29] with default FCOS parameters ($\gamma = 2$, $\alpha = 0.25$), gIoU loss[35], and the IoU prediction loss [40].

Optimization is done with AdamW [30] and 10^{-4} weight decay, and, as is standard for NFNet, adaptive gradient clipping [6] with the clipping threshold of 0.04 is used.

Backbone	Self-training	Init lr	Device	Batch size	
				LVIS _{-R}	CC12M
NFNet-F0		3×10^{-4}	16 TPUv3 chips	128	/
NFNet-F0	✓	3×10^{-4}	16 TPUv3 chips	128	1024
NFNet-F6		1×10^{-4}	16 TPUv3 chips	64	/
NFNet-F6	✓	1×10^{-4}	32 TPUv4 chips	32	256

Table 6: **Architecture-specific optimization parameters.**

Depending on the backbone architecture and whether self-training is performed, we adjust the training hardware, batch size and initial (post-warmup) learning rate – Table 6 shows the parameters for all configurations. All networks are trained for 32 epochs and the learning rate schedule consists of linear warm-up for 0.25 epochs, followed by 10 fold reductions at 67% and 89% of the training. The same schedule is used for self-training.

The implementation uses JAX [5] and the DeepMind JAX ecosystem [3].

B. Alignment preserving architecture

Figure 3 shows our alignment preserving architecture with shortcuts and trainable gates. For reference, Figure 4 shows the classic design [28, 38] of a single-stage detector.

Trainable gating. Recall that the gates perform the following operation: $o = x(1 - \tan \alpha) + y \tan \alpha$, where x and y are the inputs and α is a learnt parameter initialized to 0. We briefly experimented with the Flamingo [1] formulation: $o = x + y \tan \alpha$, and found it performs similarly.

Matching dimensionalities. For clarity of presentation, we glanced over one detail that we elaborate on here – gates and shortcuts assume the dimensionalities of all input and output features are the same, while the default design of the feature pyramid network (FPN) and detection heads includes changes in the channel dimension. We do not attempt to fix this by changing the default settings for the FPN and detector head dimensionalities and making all channels the same size, as that would increase the parameter count, be less memory and computation efficient, and be harder to compare fairly with existing approaches.

Specifically, the issue is the initial 1×1 convolution in the FPN applied on the final backbone features, as this reduces channels to 256 and thus loses information. All following processing maintains 256-D features until the very end where there is an increase back to the original dimensionality to produce classification features compatible with text embeddings (786-D and 1376-D for NFNet-F0 and NFNet-F6, respectively). We address this pragmatically – the dimensionality reduction convolution is initialized such that distances and scalar products are preserved as much as

possible, though use of an orthogonal projection. Similarly, the dimensionality increase at the end of the network is initialized to the transpose of this projection. We find that the details are not crucial – in fact the axis aligned orthogonal matrix (*i.e.* a rectangular “cropped” identity matrix) is used for simplicity, and even without this initialization the training still works well as it only needs to learn one projection to bring features back into alignment.

C. Self-training

Implementation details. Self-training simultaneously processes a batch from LVIS_{-R} with human-annotations and a batch from CC12M with pseudo-annotations. All the three losses (classification, bounding box regression, quality prediction) are used for the pseudo-labelled data as well as this performs slightly better than only using the classification loss. For Detic[†] and *Image bbox* baselines we found that, consistent with the paper [46], using only the classification loss performs best, and report only these results. The losses for the two human- and pseudo-labelled data are simply summed up, different relative weighting was not found to be beneficial for any of the methods or baselines.

Relation to other methods. We elaborate on the comparison to other methods from Section 3.3. Recall that [33, 34, 37, 48] are closed vocabulary detectors and there is no need or way to use batch-negatives. GLIPv2 [43] does not consider the zero-shot scenario and uses noun phrases instead of entire captions like we do. Furthermore, their deep fusion architecture restricts the use of batch-negatives to the pre-fusion features making its effect indirect, while our loss operates on the very final detector head classification features which are directly used for detecting the object.

In contrast to our approach and GLIPv2, Detic [46] does not make use of the image caption to produce the pseudo-detection, but instead picks the largest bounding box proposal instead. The method does use batch-negatives in an additional loss, although this is done on the global image-level rather than the bounding box-level.

Finally, the Detic paper [46] also implements baselines where the closed vocabulary pseudo-labelling methods mentioned above [33, 34, 37, 48] are adapted to the open vocabulary setting. For these baselines, the paper uses

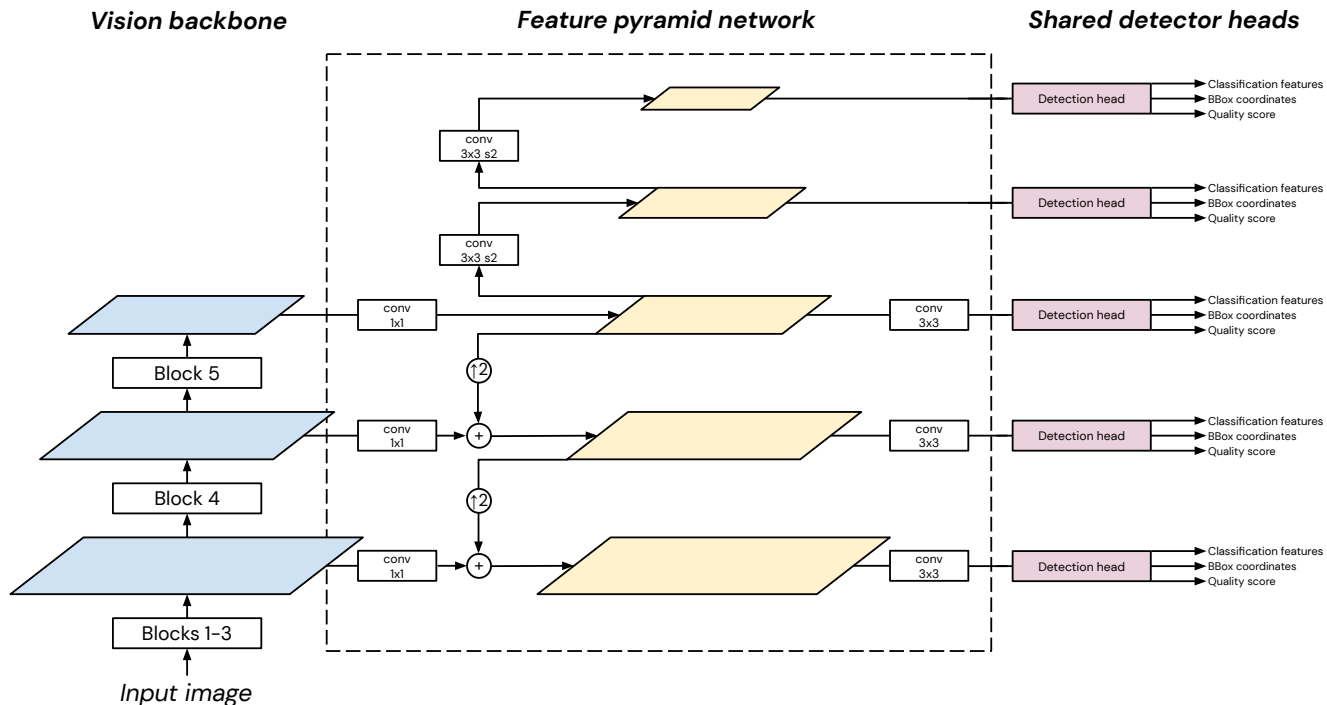


Figure 4: **Standard single-stage detector architecture.** Light blue and light yellow parallelograms represent the backbone and FPN feature maps, respectively; circles with $\uparrow 2$ are non-trainable up-sampling, squares are trainable modules (e.g. convolutions), convolution blocks show the kernel size and potential striding (‘s2’: stride 2). The alignment preserving architecture is shown in Figure 3.

the image caption to produce pseudo-detections, but does not use batch-negatives. We showed in Section 3.3.1 that batch-negatives are crucial for good performance.

Comparisons with Detic [46]. Detic [46] focuses on the zero-shot detection task but the main results forgo the open vocabulary claim as the knowledge of the names of the LVIS_R test classes is explicitly used during training, e.g. the captions are filtered for LVIS class names and this noisy label is assigned to the image. We focus on zero-shot open vocabulary detection and do not use test class names during training, so we compare only to the open vocabulary version of Detic (i.e. according to Detic terminology, no “image label” supervision, only “caption” supervision).

Furthermore, for a fair comparison as we use different backbones, detector architectures, pretraining and self-training datasets, etc, we also reimplement the open vocabulary Detic, referred to as Detic[†]. Our 3Ways approach and Detic[†] are identical everywhere apart from that pseudo-labelling is performed differently, where 3Ways uses the most confident detection produced by 2Ways given the caption, Detic[†] uses the largest bounding box proposal from 2Ways. It should be noted that our FCOS-based detector architecture is single-stage and thus technically does not have bounding box proposals, but we found that we

can simulate producing proposals by filtering out the dense boxes through thresholding the *quality score*; we sweep a range of thresholds and pick the best performing one (0.75). Our Detic[†] reimplementation surpasses the original Detic (mAP_{all} improved from 30.4% to 34.8%, and mAP_{rare} from 17.4% to 23.4%), but our 3Ways approach beats this further (mAP_{all} of 35.7% and mAP_{rare} of 25.6%).

Comparison with full LVIS training. In all other experiments detectors are trained on LVIS_R, a version of the LVIS dataset where annotations for rare classes are removed in order to test zero-shot detection. Here we investigate the value of those annotations by training a 2Ways detector on the entire LVIS (i.e. without removing annotations for rare classes). As expected, 2Ways trained on full LVIS beats 2Ways trained on LVIS_R when evaluated on LVIS itself, due its superior performance on the rare classes (Table 7). However, the effects of the dataset change are marginal when transferring to COCO and Objects365, and our self-trained 3Ways detector is still decidedly the best. Therefore, pseudo-labelled data can be more valuable than ground truth annotations. Furthermore, when using the NFNet-F0 backbone, 3Ways even beats the ‘cheating’ 2Ways on LVIS itself, but this result does not hold for the larger and better NFNet-F6 backbone.

Method	Train dataset	Backbone	LVIS		Transfer	
			mAP _{all}	mAP _{rare}	COCO	O365
2Ways	LVIS	NFNet-F0	34.4 ± 0.11	23.7 ± 1.41	40.8 ± 0.11	14.7 ± 0.07
2Ways	LVIS _R	NFNet-F0	33.8 ± 0.15	20.9 ± 0.34	40.6 ± 0.14	14.6 ± 0.04
3Ways	LVIS _R	NFNet-F0	35.7 ± 0.20	25.6 ± 1.12	41.5 ± 0.16	16.4 ± 0.15
2Ways	LVIS	NFNet-F6	45.1 ± 0.18	37.0 ± 0.97	46.5 ± 0.04	20.8 ± 0.05
2Ways	LVIS _R	NNetF-F6	43.5 ± 0.12	27.6 ± 0.80	46.5 ± 0.26	20.3 ± 0.05
3Ways	LVIS _R	NFNet-F6	44.6 ± 0.31	30.1 ± 1.83	46.9 ± 0.05	22.8 ± 0.14

Table 7: **Training on all of LVIS vs self-training.** Training 2Ways on full LVIS predictably performs better on LVIS than when training on LVIS_R (*i.e.* LVIS without annotations for rare classes). However, it loses to the self-trained detector (3Ways) when transferring to COCO and Objects365.

D. Qualitative results

Zero-shot detection. Figure 5 compares the zero-shot performance of the 2Ways and 3Ways networks – 2Ways is capable of detecting some classes not seen during training, but 3Ways is better. Figure 6 further showcases 3Ways’s zero-shot capabilities.

Random samples from benchmark datasets. Figure 7 shows detections on a sample of LVIS validation images. Transfer to COCO and Objects365 is shown in Figure 8 and 9, respectively. Kuo *et al.* [24] estimate the overlap between the training set classes of LVIS_R and the classes of COCO and Objects365 to be 91% and 63%, respectively. Therefore, Figure 9 also illustrates impressive zero-shot capabilities of our method.

Failure cases. Instead of the typical failure cases such as difficulty in detecting objects that are highly occluded, small, in unusual poses, *etc.*, here we focus on failure cases specific to zero-shot open vocabulary detection. While exhibiting impressive zero-shot performance, we observe that the network does not detect some common objects such as houses, buildings, windows, bricks, trees, leaves, rocks, eyes, *etc.* We speculate that this is because images containing these objects are often seen during training but never annotated with a bounding box, thus the network learns they are not-an-object and does not assign a high enough quality score. There is also the philosophical question of what is an object, for example, object parts such as eyes generally do not get detected by our networks. However, the system does detect wheels, as they are annotated in the LVIS_R training set. All of the above indicates that there is room for improvement in the zero-shot capabilities of the objectness component of detectors (‘quality score’ here, region proposal networks in two-stage detectors), or that this concept should be removed completely as being somewhat incompatible with zero-shot open vocabulary detection.

Image attribution. Images used in Figure 1, 5 and 6 were downloaded from Wikimedia or are personal photos

of an author (Relja Arandjelović) and all are free to use and modify – we made no modifications apart from resolution change and the overlaying of the detections. The Wikimedia originals can be found at the following links:

[https://commons.wikimedia.org/wiki/File:Parisian_gargoyle_\(Unsplash\).jpg](https://commons.wikimedia.org/wiki/File:Parisian_gargoyle_(Unsplash).jpg)
https://commons.wikimedia.org/wiki/File:Venezia-gondola_on_canal_grande.JPG
https://commons.wikimedia.org/wiki/File:Macaroons_at_Smiths.jpg
https://commons.wikimedia.org/wiki/File:Round_hay_bales_and_a_hot_air_none
↔ [balloon_somewhere_in_Luxembourg.jpg](#)
https://commons.wikimedia.org/wiki/File:POOL_HALL_-_NARA_-_543975.jpg
https://commons.wikimedia.org/wiki/File:Jumping_over_the_moon.jpg
https://commons.wikimedia.org/wiki/File:Wolves_chasing_a_wapiti,_none
↔ [Yellowstone_River_\(2\).jpg](#)
https://commons.wikimedia.org/wiki/File:2020-01-11_Men's_Ice_hockey_3x3_none
↔ [Preliminary_round_Team_Blue_vs._Team_Orange_\(2020_Winter_Youth_none](#)
↔ [Olympics\)_by_Sandro_Halank\(057\).jpg](#)

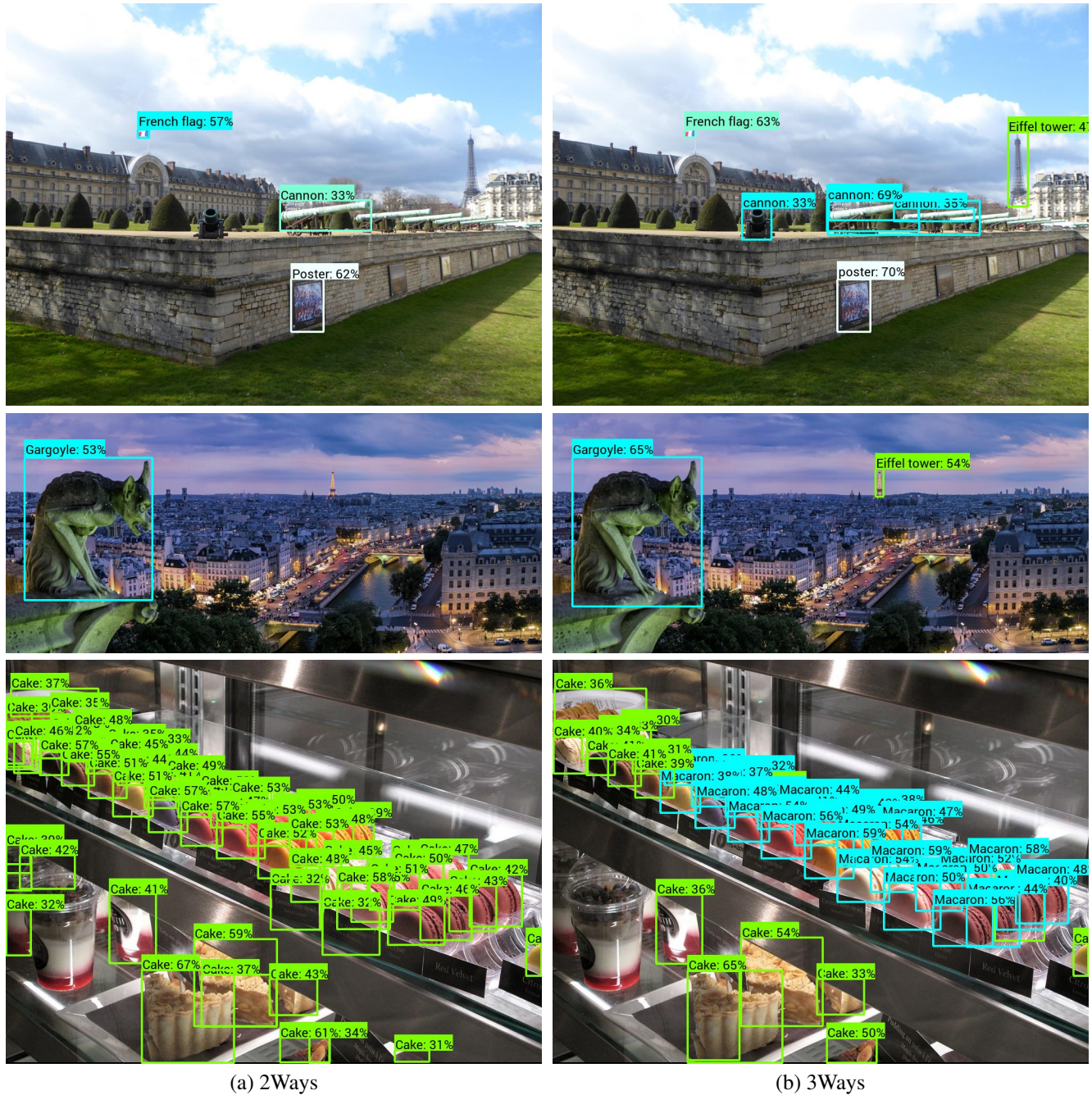


Figure 5: *2Ways* vs *3Ways* (NFNet-F6). Detections with a score larger than 0.3 are shown. The queries for the three examples are: (top) Eiffel tower, French flag, cannon, poster; (middle) Eiffel tower, gargoyle; (bottom) cake, macaron. No human-annotated boxes were seen during training for all queries apart from poster and cake. *2Ways* has zero-shot detection capability, but *3Ways* generally outperforms it.

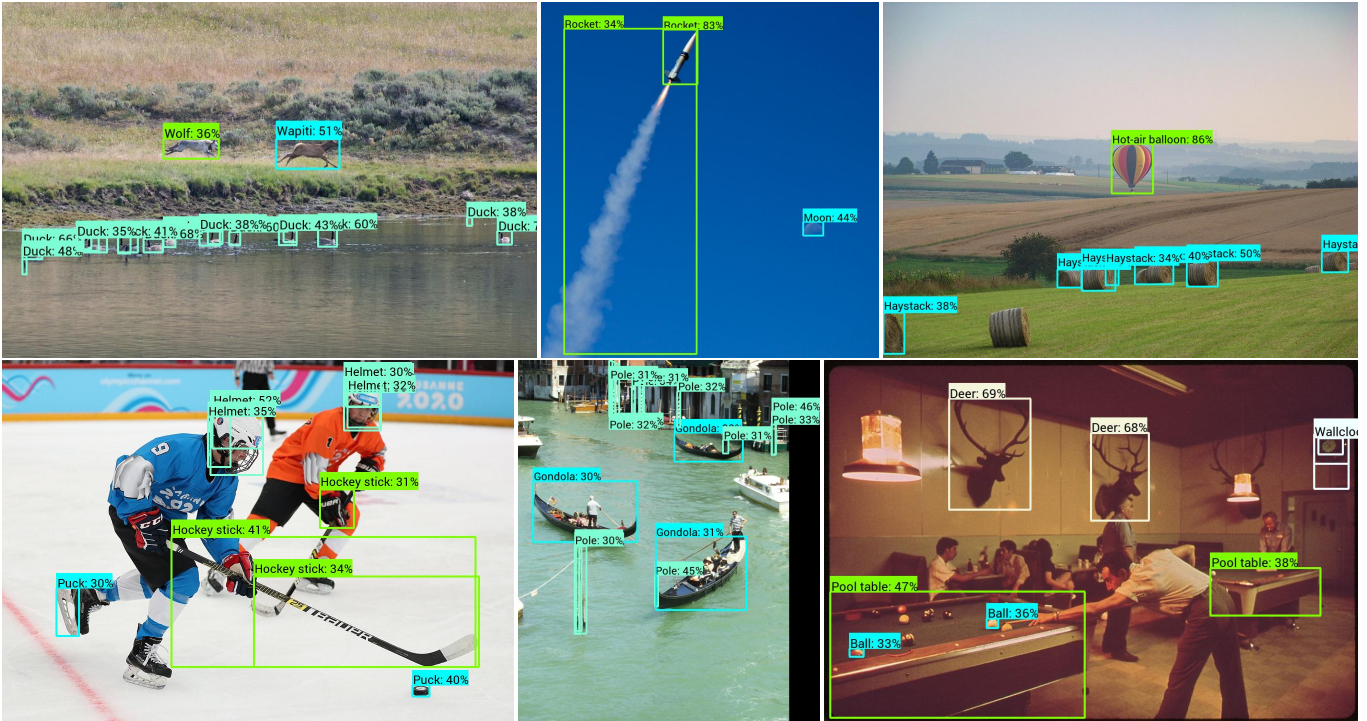


Figure 6: *3Ways* (NFNet-F6) zero-shot detection examples. Detections with a score larger than 0.3 are shown. The queries for the six examples are: (top-left) **wolf**, **wapiti**, **duck**; (top-middle) **rocket**, **moon**; (top-right) **hot-air balloon**, **haystack**; (bottom-left) **helmet**, **puck**, **hockey stick**; (bottom-middle) **gondola**, **pole**; (bottom-right) **pool table**, **ball**, **deer**, **wallclock**. Networks were trained with human-annotated boxes for **duck**, **helmet**, **pole**, **ball**, **deer** and **wallclock**, while no human-annotated boxes were seen during training for **wolf**, **wapiti**, **rocket**, **moon**, **hot-air balloon**, **haystack**, **puck**, **hockey stick**, **gondola**, and **pool table**. Note that **dog** (a frequent training category) rightfully has a lower confidence than **wolf** for the top-left image.

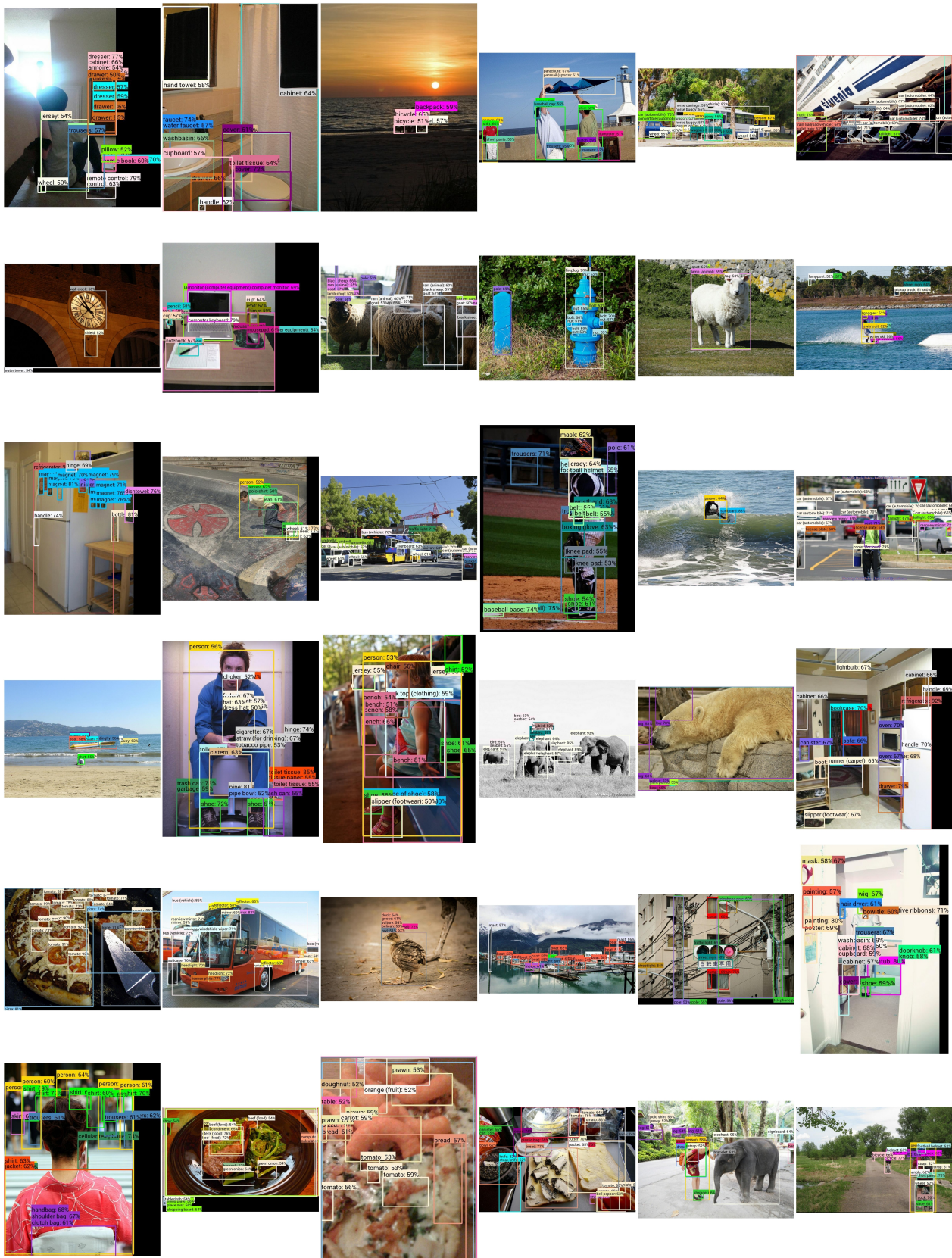


Figure 7: Random sample: LVIS validation set (3Ways, NFNet-F6). Up to 20 detections with a score larger than 0.5 are shown. Best viewed digitally.

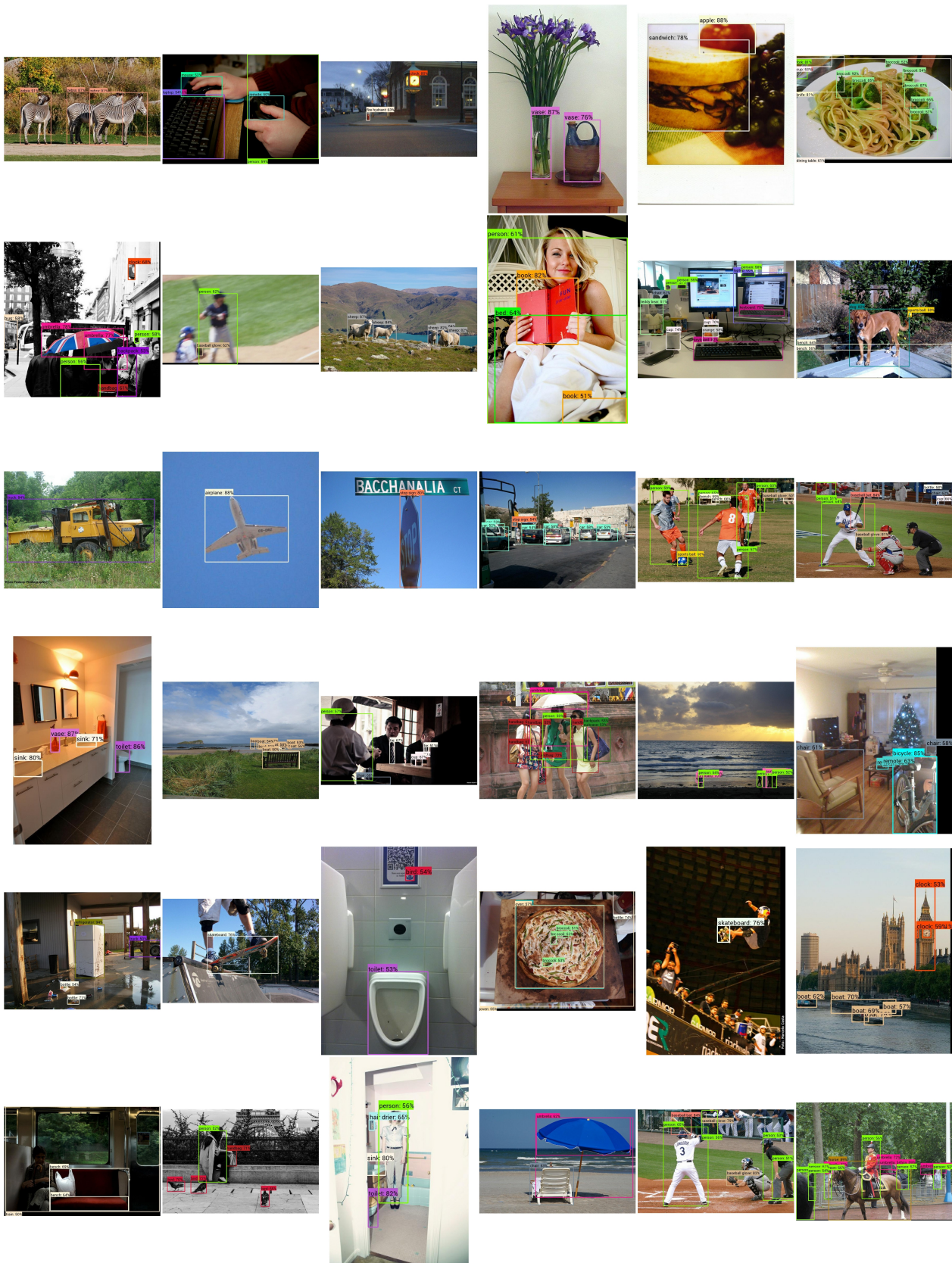


Figure 8: **Random sample: COCO validation set (3Ways, NfNet-F6)**. The detector is trained on LVIS_R and transferred to COCO without any additional training. Up to 20 detections with a score larger than 0.5 are shown. Best viewed digitally.

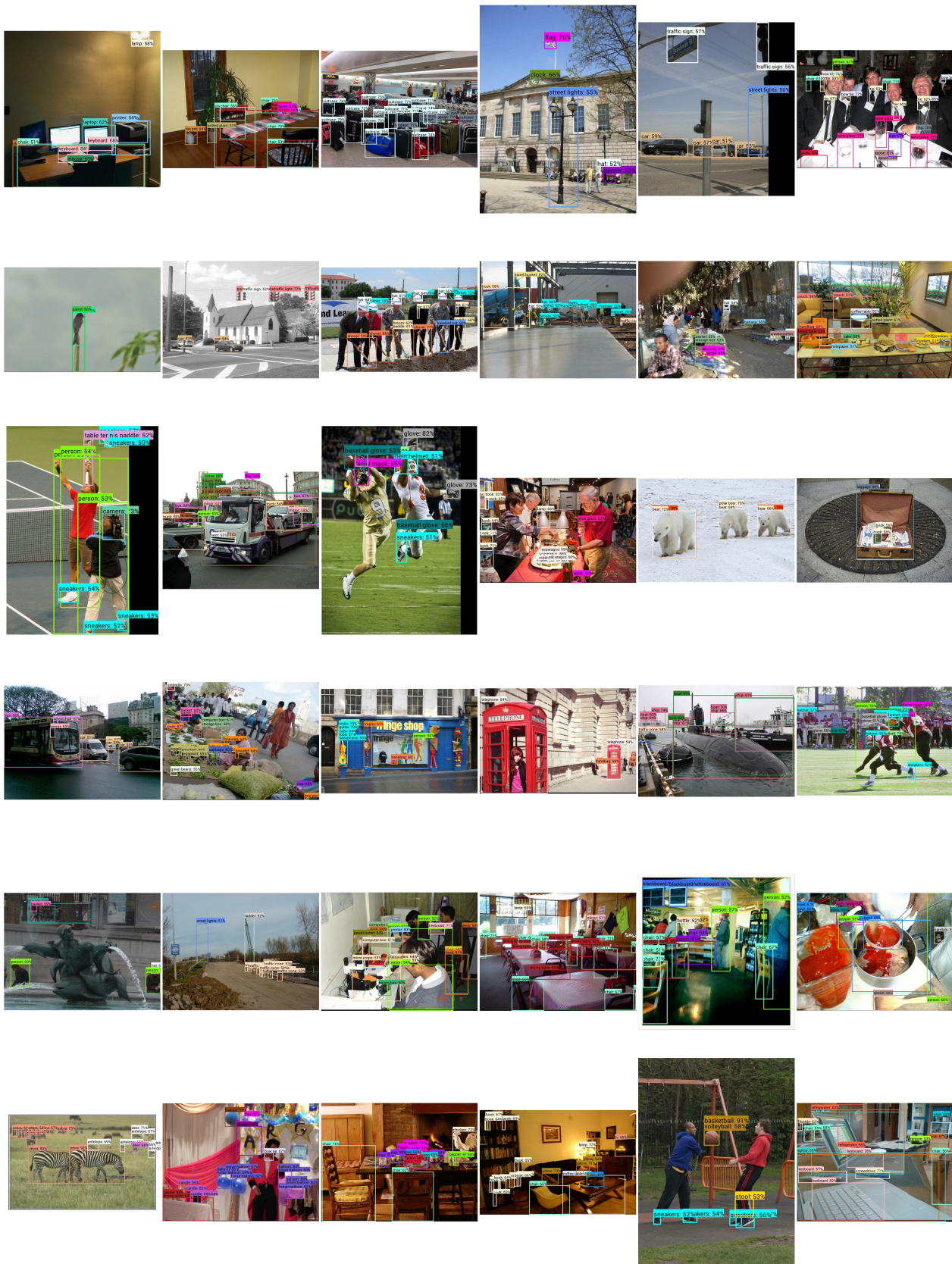


Figure 9: **Random sample: Objects365-v1 validation set (3Ways, NFNet-F6).** The detector is trained on LVIS_R and transferred to Objects365 without any additional training. Up to 20 detections with a score larger than 0.5 are shown. Best viewed digitally.